Enhanced nonlinear optics in photonic-crystal microcavities

Jorge Bravo-Abad, Alejandro Rodriguez, Peter Bermel , Steven G. Johnson, John D. Joannopoulos, and Marin Soljačić

Physics Department and Research Laboratory of Electronics, MIT, Cambridge, MA 02139, USA

Abstract: Nonlinear photonic-crystal microresonators offer unique fundamental ways of enhancing a variety of nonlinear optical processes. This enhancement improves the performance of nonlinear optical devices to such an extent that their corresponding operation powers and switching times are suitable for their implementation in realistic ultrafast integrated optical devices. Here, we review three different nonlinear optical phenomena that can be strongly enhanced in photonic crystal microcavities. First, we discuss a system in which this enhancement has been successfully demonstrated both theoretically and experimentally, namely, a photonic crystal cavity showing optical bistability properties. In this part, we also present the physical basis for this dramatic improvement with respect to the case of traditional nonlinear devices based on nonlinear Fabry-Perot etalons. Secondly, we show how nonlinear photonic crystal cavities can be also used to obtain complete second-harmonic frequency conversion at very low input powers. Finally, we demonstrate that the nonlinear susceptibility of materials can be strongly modified via the so-called Purcell effect, present in the resonant cavities under study.

OCIS codes: (190.2620) Nonlinear optics: frequency conversion; (230.4320) Nonlinear optical devices

References and links

1. R. W. Boyd, *Nonlinear Optics* (Academic Press, California, 1992).
2. H. M. Gibbs, *Optical Bistability: Controlling Light with Light* (Academic Press, Orlando, FL, 1985).
3. For a review on this topic, see K. J. Vahala, "Optical microcavities," Nature **424**, 839–846 (2003).
4. J. D. Joannopoulos, R. D. Meade, and J. N. Winn, *Photonic Crystals: Molding the Flow of Light* (Princeton Univ. Press, 1995).
5. J. S. Foresi, P. R. Villeneuve, J. Ferrera, E. R. Thoen, G. Steinmeyer, S. Fan, J. D. Joannopoulos, L. C. Kimerling, H. I. Smith, and E. P. Ippen, "Photonic-bandgap microcavities in optical waveguides," Nature **390**, 143–145 (1997).
6. S. Fan, P. R. Villeneuve, J. D. Joannopoulos, and H. A. Haus, "Channel drop tunneling through localized states," Phys. Rev. Lett. **80**, 960–963 (1998).
7. O. Painter, J. Vuckovic, and A. Scherer, "Defect modes of a two-dimensional photonic crystal in an optically thin dielectric slab," J. Opt. Soc. Am. B **16**, 275–285 (1999).
8. S. Noda, A. Chutinan, and M. Imada, "Trapping and emission of photons by a single defect in a photonic bandgap structure," Nature **407**, 608–610 (2000).
9. S. G. Johnson, S. Fan, A. Mekis, and J. D. Joannopoulos, "Multipole-cancellation mechanism for high-Q cavities in the absence of a complete photonic band gap," Appl. Phys. Lett. **78**, 3388–3390 (2001).
10. T. Yoshie, J. Vuckovic, A. Scherer, H. Chen, and D. Deppe, "High quality two-dimensional photonic crystal slab cavities," Appl. Phys. Lett. **79**, 4289–4291 (2001).
11. J. Vuckovic, M. Loncar, H. Mabuchi, and A. Scherer, "Design of photonic crystal microcavities for cavity QED," Phys. Rev. E **65**, 016608 (2002).

#87210 - $15.00 USD Received 4 Sep 2007; revised 12 Nov 2007; accepted 12 Nov 2007; published 21 Nov 2007

12. Y. Akahane, T. Asano, B. S. Song, and S. Noda), "Investigation of high-Q channel drop filters using donor-type defects in two-dimensional photonic crystal slabs," Appl. Phys. Lett. **83**, 1512–1514 (2003).
13. K. Srinivasan, P. E. Barclay, O. Painter, J. X. Chen, A. Y. Cho, and C. Gmachl, "Experimental demonstration of a high quality factor photonic crystal microcavity," Appl. Phys. Lett. **83**, 1915–1917 (2003).
14. H. Y. Ryu, M. Notomi, and Y. H. Lee, "High-quality-factor and small-mode-volume hexapole modes in photonic-crystal-slab nanocavities," Appl. Phys. Lett. **83**, 4294–4296 (2003).
15. A. Rodriguez, M. Ibanescu, J. D. Joannopoulos, and S. G. Johnson, "Disorder-immune confinement of light in photonic-crystal cavities," Opt. Lett. **30**, 3192–3194 (2005).
16. S. Noda, M. Fujita, and T. Asano, "Spontaneous-emission control by photonic crystals and nanocavities," Nature Phot. **1**, 449–458 (2007).
17. E. Centeno and D. Felbacq, "Optical bistability in finite-size nonlinear bidimensional photonic crystals doped by a microcavity," Phys. Rev. B **62**, R7683–R7686 (2000).
18. M. Soljacic, S. G. Johnson, S. Fan, M. Ibanescu, E. Ippen, and J. D. Joannopoulos, "Photonic-crystal slow-light enhancement of non-linear phase sensitivity," J. Opt. Soc. Am. B **19**, 2052–2059 (2002).
19. M. Soljacic, M. Ibanescu, S. G. Johnson, Y. Fink, and J. D. Joannopoulos, "Optimal bistable switching in non-linear photonic crystals," Phys. Rev. E **66**, 055601(R) (2002).
20. S. F. Mingaleev and Y. S. Kivshar, "Nonlinear transmission and light localization in photonic crystal waveguides," J. Opt. Soc. Am. B **19**, 2241–2249 (2002).
21. A. R. Cowan and J. F. Young, "Optical bistability involving photonic crystal microcavities and Fano line shapes," Phys. Rev. E **68**, 046606 (2003).
22. M. Soljacic, C. Luo, J. D. Joannopoulos, and S. Fan, "Nonlinear photonic crystal microdevices for optical integration," Opt. Lett. **28**, 637–639 (2003).
23. M. Soljacic, M. Ibanescu, S. G. Johnson, J. D. Joannopoulos, and Y. Fink, "Optical bistability in axially modulated OmniGuide fibers," Opt. Lett. **28**, 516–518 (2003).
24. M. F. Yanik, S. Fan, and M. Soljacic, "High-contrast all-optical bistable switching in photonic crystal microcavities," Appl. Phys. Lett. **83**, 2739–2741 (2003).
25. M. F. Yanik, S. Fan, M. Soljacic, and J. D. Joannopoulos, "All-optical transistor action with bistable switching in a photonic crystal cross-waveguide geometry," Opt. Lett. **28**, 2506–2508 (2003).
26. J. Trull, R. Vilaseca, J. Martorell, and R. Corbalan, "Second-harmonic generation in local modes of a truncated periodic structure," Opt. Lett. **20**, 1746–1748 (1995).
27. T. V. Dolgova, A. I. Maidykovski, M. G. Martemyanov, A. A. Fedyanin, O. A. Aktsipetrov, G. Marowsky, V. A. Yakovlev, G. Mattei, N. Ohta, and S. Nakabayashi, "Giant optical second-harmonic generation in single and coupled microcavities formed from one-dimensional photonic crystals," J. Opt. Soc. Am. B **19**, 2129–2140 (2002).
28. F. F. Ren, R. Li, C. Cheng, and H. T. Wang, J. R. Qiu, J. H. Si, and K. Hirao, "Giant enhancement of second harmonic generation in a finite photonic crystal with a single defect and dual-localized modes," Phys. Rev. B **70**, 245109 (2004).
29. M. G. Martemyanov, E. M. Kim, T. V. Dolgova, A. A. Fedyanin, O. A. Aktsipetrov, and G. Marowsky, "Third-harmonic generation in silicon photonic crystals and microcavities," Phys. Rev. B **70**, 073311 (2004).
30. M. Soljacic and J. D. Joannopoulos, "Enhancement of nonlinear effects using photonic crystals," Nature Mater. **3**, 211–219 (2004).
31. P. E. Barclay, K. Srinivasan, and O. Painter, "Nonlinear response of silicon photonic crystal microresonators excited via an integrated waveguide and fiber taper," Opt. Express **13**, 801–820 (2005).
32. T. Tanabe, M. Notomi, S. Mitsugi, A. Shinya, and E. Kuramochi, "Fast bistable all-optical switch and memory on a silicon photonic crystal on-chip," Opt. Lett. **30**, 2575–2577 (2005).
33. M. Notomi, A. Shinya, S. Mitsugi, G. Kira, E. Kuramochi, and T. Tanabe, "Optical bistable switching action of Si high-*Q* photonic-crystal nanocavities," Opt. Express **13**, 2678–2687 (2005).
34. F. F. Ren, R. Li, C. Cheng, J. Chen, Y. X. Fan, J. P. Ding, and H. T. Wang, "Low-threshold and high-efficiency optical parametric oscillator using a one-dimensional single-defect photonic crystal with quadratic nonlinearity," Phys. Rev. B **73**, 033104 (2006).
35. A. Rodriguez, M. Soljacic, J. D. Joannopoulos, and S. G. Johnson, "$\chi^{(2)}$ and $\chi^{(3)}$ harmonic generation at a critical power in inhomogeneous doubly resonant cavities," Opt. Express **15**, 7303–7318 (2007).
36. P. Bermel, A. Rodriguez, J. D. Joannopoulos, and M. Soljacic, "Tailoring optical nonlinearities via the Purcell effect," Phys. Rev. Lett. **99**, 053601 (2007).
37. A. Taflove and S. C. Hagness, *Computational Electrodynamics: The Finite-Difference Time-Domain Method* (Artech, Norwood, MA, 2000).
38. H. A. Haus, *Waves and Fields in Optoelectronics* (Prentice-Hall, Englewood Cliffs, NJ, 1984).
39. J. Bravo-Abad, S. Fan, S. G. Johnson, J. D. Joannopoulos, and M. Soljacic, "Modeling nonlinear optical phenomena in nanophotonics," J. Lightwave Technol. **25**, 2539–2546 (2007).
40. A. Farjadpour, D. Roundy, A. Rodriguez, M. Ibanescu, P. Bermel, J. D. Joannopoulos, S. G. Johnson, and G. W. Burr "Improving accuracy by subpixel smoothing in the finite-difference time domain," Opt. Lett. **31**, 2972–2974 (2006).
41. G. D'Aguanno, M. Centini, M. Scalora, C. Sibilia, Y. Dumeige, P. Vidakovic, J. A. Levenson, M. J. Bloemer,

#87210 - $15.00 USD Received 4 Sep 2007; revised 12 Nov 2007; accepted 12 Nov 2007; published 21 Nov 2007

C. M. Bowden, J. W. Haus, and M. Bertolotti, "Photonic band edge effects in finite structures and applications to $\chi^{(2)}$ interactions," Phys. Rev. E **64**, 016609 (2001).
42. M. L. Povinelli, S. G. Johnson, and J. D. Joannopoulos, "Slow-light, band-edge waveguides for tunable time delays," Opt. Express **13**, 7145–7159 (2005).
43. Y. Xu, R. K. Lee, and A. Yariv, "Propagation and second-harmonic generation of electromagnetic waves in a coupled-resonator optical waveguide," J. Opt. Soc. Am. B **17**, 387–400 (2000).
44. J. E. Heebner, R. W. Boyd, and Q. H. Park, "Slow light, induced dispersion, enhanced nonlinearity, and optical solitons in a resonator-array waveguide," Phys. Rev. E **65**, 036619 (2002).
45. V_{MODE} is actually the effective modal volume (weighted by local $\chi^{(3)}$) but it is quantitatively very similar to the usual definition of modal volume.
46. M. Notomi, Personal communication (2007).
47. Q. F. Xu and M. Lipson, "Carrier-induced optical bistability in Silicon ring resonators," Opt. Lett. **31**, 341–343 (2006).
48. S. Pearl, H. Lotem, Y. Shimony, and S. Rosenwaks, "Optimization of laser intracavity second-harmonic generation by a linear dispersion element," J. Opt. Soc. Am. B **16**, 1705–1711 (1999).
49. A. V. Balakin, V. A. Bushuev, B. I. Mantsyzov, I. A. Ozheredov, E. V. Petrov, A. P. Shkurinov, P. Masselin, and G. Mouret, "Enhancement of sum frequency generation near the photonic band edge under the quasiphase matching condition," Phys. Rev. E **63**, 046609 (2001).
50. A. H. Norton and C. M. de Sterke, "Optimal poling of nonlinear photonic crystals for frequency conversion," Opt. Lett. **28**, 188–190 (2003).
51. G. D' Aguanno, M. Centini, M. Scalora, C. Sibilia, M. Bertolotti, M. J. Bloemer, and C. M. Bowden, "Generalized coupled-mode theory for $\chi^{(2)}$ interactions in finite multi-layered structures," J. Opt. Soc. Am. B **19**, 2111–2121 (2002).
52. A. R. Cowan and J. F. Young, "Mode matching for second-harmonic generation in photonic crystal waveguides," Phys. Rev. E **65**, 085106 (2002).
53. A. M. Malvezzi, G. Vecchi, M. Patrini, G. Guizzetti, L. C. Andreani, F. Romanato, L. Businaro, E. Di Fabrizio, A. Passaseo, and M. De Vittorio, "Resonant second-harmonic generation in a GaAs photonic crystal waveguide," Phys. Rev. B **68**, 161306 (2003).
54. P. P. Markowicz, H. Tiryaki, H. Pudavar, P. N. Prasad, N. N. Lepeshkin, and R. W. Boyd, "Dramatic enhancement of third-harmonic generation in three-dimensional photonic crystals," Phys. Rev. Lett. **92**, 083903 (2004).
55. V. Berger, "Second-harmonic generation in monolithic cavities," J. Opt. Soc. Am. B **14**, 1351–1360 (1997).
56. Y. Dumeige and P. Feron, "Wispering-gallery-mode analysis of phase-matched doubly resonant second-harmonic generation," Phys. Rev. A **74**, 063804 (2006).
57. J. A. Armstrong, N. Bloembergen, J. Ducuing, and P. S. Pershan, "Interactions between light waves in a nonlinear dielectric," Phys. Rev. **127**, 1918–1939 (1962).
58. A. Ashkin, G. Boyd, and J. M. Dziedzic, "Resonant optical second harmonic generation and mixing," IEEE J. Quantum Electron. **2**, 109–124 (1966).
59. R. Smith, "Theory of intracavity optical second-harmonic generation," IEEE J. Quantum Electron. **6**, 215–223 (1970).
60. A. Ferguson and M. Dunn, "Intracavity second harmonic generation in continuous-wave dye lasers," IEEE J. Quantum Electron. **13**, 751–756 (1977).
61. M. Brieger, H. Busener, A. Hese, F. V. Moers, and A. Renn, "Enhancement of single frequency SHG in a passive ring resonator," Opt. Commun. **38**, 423–426 (1981).
62. J. C. Bergquist, H. Hemmati, and W. M. Itano, "High power second harmonic generation of 257 nm radiation in an external ring cavity," Opt. Comm. **43**, 437–442 (1982).
63. W. J. Kozlovsky, W. P. Risk, W. Lenth, B. G. Kim, G. L. Bona, H. Jaeckel, and D. J. Webb, "Blue light generation by resonator-enhanced frequency doubling of an extended-cavity diode laser," Appl. Phys. Lett. **65**, 525–527 (1994).
64. G. J. Dixon, C. E. Tanner, and C. E. Wieman, "432-nm source based on efficient second-harmonic generation of GaAlAs diode-laser radiation in a self-locking external resonant cavity," Opt. Lett. **14**, 731–733 (1989).
65. M. J. Collett and R. B. Levien, "Two-photon loss model of intracavity second-harmonic generation," Phys. Rev. A **43**, 5068–5072 (1991).
66. M. A. Persaud, J. M. Tolchard, and A. I. Ferguson, "Efficient generation of picosecond pulses at 243 nm," IEEE J. Quantum Electron. **26**, 1253–1258 (1990).
67. Z. Y. Ou and H. J. Kimble, "Enhanced conversion efficiency for harmonic generation with double resonance," Opt. Lett. **18**, 1053–1055 (1993).
68. G. T. Moore, K. Koch, and E. C. Cheung, "Optical parametric oscillation with intracavity second-harmonic generation," Opt. Commun. **113**, 463–470 (1995).
69. K. Schneider, S. Schiller, J. Mlynek, M. Bode, and I. Freitag, "1.1-W single-frequency 532-nm radiation by second-harmonic generation of a miniature Nd:YAG ring laser," Opt. Lett. **21**, 1999–2001 (1996).
70. X. Mu, Y. J. Ding, H. Yang, and G. J. Salamo, "Cavity-enhanced and quasiphase-matched mutli-order reflection-second-harmonic generation from GaAs/AlAs and GaAs/AlGaAs multilayers," Appl. Phys. Lett. **79**, 569–571

#87210 - $15.00 USD Received 4 Sep 2007; revised 12 Nov 2007; accepted 12 Nov 2007; published 21 Nov 2007

(2001).
71. J. Hald, "Second harmonic generation in an external ring cavity with a Brewster-cut nonlinear cystal: theoretical considerations," Opt. Commun. **197**, 169–173 (2001).
72. G. McConnell, A. I. Ferguson, and N. Langford, "Cavity-augmented frequency tripling of a continuous wave mode-locked laser," J. Phys. D: Appl.Phys **34**, 2408–2413 (2001).
73. T. M. Liu, C. T. Yu, and C. K. Sun, "2 Ghz repetition-rate femtosecond blue sources by second-harmonic generation in a resonantly enhanced cavity," Appl. Phys. Lett. **86**, 061112 (2005).
74. L. Scaccabarozzi, M. M. Fejer, Y. Huo, S. Fan, X. Yu, and J. S. Harris, "Enhanced second-harmonic generation in AlGaAs/Al_xO_y tightly confining waveguides and resonant cavities," Opt. Lett. **31**, 3626–3628 (2006).
75. A. Di Falco, C. Conti, and G. Assanto, "Impedance matching in photonic crystal microcavities for second-harmonic generation," Opt. Lett. **31**, 250–252 (2006).
76. K. Koch and G. T. Moore, "Singly resonant cavity-enhanced frequency tripling," J. Opt. Soc. Am. B **16**, 448–459 (1999).
77. E. M. Purcell, "Spontaneous emission probabilities at radio frequencies," Phys. Rev. **69**, 681–686 (1946).
78. D. Kleppner, "Inhibited spontaneous emission," Phys. Rev. Lett. **47**, 233–236 (1981).
79. H. Y. Ryu and M. Notomi, "Enhancement of spontaneous emission from the resonant modes of a photonic crystal slab single-defect cavity," Opt. Lett. **28**, 2390–2392 (2003).
80. P. Bermel, J. D. Joannopoulos, Y. Fink, P. A. Lane, and C. Tapalian, "Properties of radiating pointlike sources in cylindrical omnidirectionally reflecting waveguides," Phys. Rev. B **69**, 035316 (2004).
81. D. Englund, D. Fattal, E. Waks, G. Solomon, B. Zhang, T. Nakaoka, Y. Arakawa, Y. Yamamoto, and J. Vuckovic, "Controlling the spontaneous emission rate of single quantum dots in a two-dimensional photonic crystal," Phys. Rev. Lett. **95**, 013904 (2005).
82. S. John and T. Quang, "Resonant nonlinear dielectric response in a photonic band gap material," Phys. Rev. Lett. **76**, 2484–2487 (1996).
83. D. Miller, S. Smith, and B. Wherrett, "The microscopic mechanism of 3rd-order optical nonlinearity in InSb," Opt. Commun. **35**, 221–226 (1980).
84. M. Nielsen and I. Chuang, *Quantum Computation and Quantum Information* (Cambridge University Press, Cambridge, England, 2000).
85. J. J. Sakurai, *Modern Quantum Mechanics* (Addison-Wesley, Reading, MA, 1994).
86. G. Lenz, J. Zimmermann, T. Katsufuji, M. E. Lines, H. Y. Hwang, S. Spalter, R. E. Slusher, S. W. Cheong, J. S. Sanghera, and I. D. Aggarwal, "Large Kerr effect in bulk Se-based chalcogenide glasses," Opt. Lett. **25**, 254–256 (2000).
87. V. Savona, L. C. Andreani, P. Schwendimann, and A. Quattropani, "Quantum well excitons in semiconductor microcavities: unified treatment of weak and strong coupling regimes", Solid State Comm. **93**, 733–739 (1995).
88. X. Brokmann, L. Coolen, M. Dahan, and J. P. Hermier, "Measurement of the radiative and nonradiative decay rates of single CdSe nanocrystals through a controlled modification of their spontaneous emission," Phys. Rev. Lett. **93**, 107403 (2004).
89. H. Shinojima, "Optical nonlinearity in CdSSe microcrystallites embedded in glasses," IEICE Trans. Electron. **E90-C**, 127–134 (2007).
90. D. V. Talapin, A. L. Rogach, A. Kornowski, M. Haase, and H. Weller, "Highly luminescent monodisperse CdSe and CdSe/ZnS nanocrystals synthesized in a hexadecylamine-trioctylphosphine oxide-trioctylphospine mixture," Nano Lett. **1**, 207–211 (2001).
91. N. M. Litchinitser, A. Abeeluck, C. Headley, and B. Eggleton, "Antiresonant reflecting photonic crystal optical waveguides," Opt. Lett. **27**, 1592–1594 (2002).

1. Introduction

Since the early days of nonlinear optics, optical resonators have been seen as an attractive way to enhance nonlinear optical phenomena, such as a frequency conversion processes [1] (in optical parametric oscillators) or optical bistability properties [2]. Traditionally, these nonlinear optical resonators have consisted of a nonlinear material located between two partially transmitting mirrors. Although interesting in their own right, the application of these nonlinear Fabry-Perot interferometers for designing all-optical logical devices is rather limited, as they can not fulfill the requirements in size, switching time and operating power of practical integrated optical systems.

On a separate front, the rapid development of fabrication techniques at micro and nanometric scale has enabled the successful demonstration of optical micro- and nano-cavities where light is strongly confined in a very small volume. This corresponds to the case where the ratio between the quality factor Q and the modal volume V_{MODE} is extremely large, such that

#87210 - $15.00 USD Received 4 Sep 2007; revised 12 Nov 2007; accepted 12 Nov 2007; published 21 Nov 2007

$Q/V_{MODE} >> 1/\lambda^3$). Here, it is important to emphasize that the modal volume is a measure of the spatial extent of the mode in the material of interest, but its precise definition will depend on the physical phenomenon of interest (for example, as it is shown in this work, there are different relevant definitions of the modal volume for Kerr bistability, harmonic generation or Purcell enhancement).

During the last decade, different types of optical cavities characterized by ultrasmall modal volumes and extremely high quality factors have been sucessfully demonstrated (such as photonic-crystal (PhC) cavities or microtoroid and microsphere resonators, just to cite some examples [3]). Among them, due to their unique confinement mechanism [4], PhCs cavities have proven to be a versatile route to develop novel optical integrated devices. PhC optical cavities are usually created by introducing a small defect in an otherwise perfectly periodically modulated refractive index profile in either one, two or three dimensions. The linear properties of PhCs including such defects have been extensively studied both theoretically and experimentally [5–15]. Recently, it has been experimentally demonstrated that it is possible to design PhC microcavities with quality factors of $Q \sim 10^6$ and modal volumes of the order of a cubic wavelength [16].

As a consequence of these recent advances in nanophotonic fabrication, many of the nonlinear phenomena previously analyzed in conventional nonlinear etalons are being revisited within the context of PhC cavities [17–40]. Although it is true that the physical mechanisms producing nonlinear phenomena (such as optical bistability or nonlinear frequency conversion) in PhC cavities are similar to those observed in their conventional counterparts, it has been demonstrated that PhC microresonators enhance the performance of traditional nonlinear devices by several orders of magnitude. In addition, due to their design versatility, PhC cavities can be used as the basis of completely new configurations performing all-optical logic functions, such as all-optical transistor action [25]. Moreover, PhC resonators offer new fundamental ways of tailoring optical nonlinearities by using the so-called Purcell effect. Finally, in this context, note that not only PhC resonators can lead to a strong enhancement of nonlinear phenomena, but also nonlinear effects can be enhanced by using slow-light properties of PhCs, via the corresponding band egdes [41, 42] or by means of coupled-cavity waveguides [18, 43, 44]

It is important to mention that, together with the aforementioned rapid development of the experimental techniques, during the last decade there has also been an important growth in large-scale computing technologies. Thus, the combination of pure numerical methods as the non-linear finite-difference-time domain method (FDTD) [37] (which simulates Maxwell's equations with no approximation apart from discretization), with analytical approaches such as coupled-mode theory [38] or perturbation theory [19] allow a complete characterization of the electromagnetic response of the nonlinear PhC cavities under study. In particular, all the theoretical calculations shown in this paper have been obtained by using one of the tools just mentioned. However, since this work is mainly focused in explaining the physical mechanisms responsible for the observed results, we refer to the reader to more specialized references for details on the numerical calculations and analysis [37–40].

This manuscript reviews three examples of nonlinear optical processes that can be dramatically enhanced by PhC resonators. The first example in Section 2 reviews the mechanism of optical bistability, and shows how PhC cavities enhance it in a striking fashion. The second example in Section 3 shows how PhCs can dramatically lower the threshold for 100% efficient harmonic generation compared to conventional approaches. The third example in Section 4 models the origin of nonlinearity at an atomic level, and shows how it can be tailored by its PhC enviroment. In particular, it gives rise to PhC cavities that enhance not only the field but also the nonlinear coefficient. These results are summarized in Section 5.

#87210 - $15.00 USD Received 4 Sep 2007; revised 12 Nov 2007; accepted 12 Nov 2007; published 21 Nov 2007

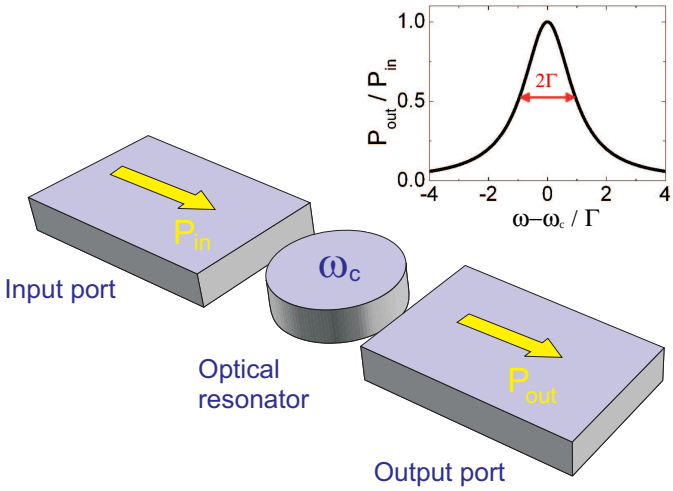

Fig. 1. Sketch of a system composed by an optical resonator coupled symmetrically to both an input and output ports. ω_c is the corresponding resonant frequency and Γ is the width of the resonance. P_{in} and P_{out} label the incoming and outgoing powers through the structure, respectively. Inset shows the typical linear transmission spectrum corresponding to this system.

2. Optical bistability in photonic crystal cavities

For pedagogical reasons, let us start by considering the general system sketched in Fig. 1. It consists of a resonant nonlinear cavity coupled to both an input and an output port. This optical resonator can be a conventional nonlinear Fabry-Perot resonator (i.e., a slab of nonlinear material situated between two partially transmitting mirrors) as well as a PhC microcavity (a defect in an otherwise perfectly periodic PhC). In the linear regime, light is transmitted between the input and the output ports by means of a resonant tunneling process. Thus, if we assume that the input and output ports are two single-mode waveguides, the ratio between the input and outgoing powers (P_{in} and P_{out}, respectively) is characterized by a Lorentzian shape (see inset of Fig. 1)

$$\frac{P_{out}}{P_{in}} = \frac{1}{1+((\omega-\omega_c)/\Gamma)^2} \tag{1}$$

where Γ is the width of the resonance and ω_c is the corresponding resonant frequency. Note that from Γ and ω_c we can obtain the quality factor of the cavity $Q = \omega_c/2\Gamma$.

Now, let us consider how this behavior changes when, by means of some physical mechanism, we induce a nonlinear response in the optical resonator. For definiteness, we assume that in our system the nonlinearity is introduced by a Kerr-like nonlinear material inside the resonator. In this way, we are introducing into our problem a change of the refractive index of the optical resonator δn, so that $\delta n \propto n_2|\mathbf{E}|^2$, with $\mathbf{E}$ being the electric field inside the resonator and n_2 the Kerr coefficient. Imagine next that we illuminate the cavity with light at a frequency ω_p detuned below the resonant frequency ω_c of the cavity by several times the resonant width (we define $\delta\omega = \omega_c - \omega_p$, see vertical black line in Fig. 2(a)). In the linear regime, this will correspond to a low value of the ratio P_{out}/P_{in} (see black arrow in Fig. 2(a)). Consider now the effect introduced by an increase δn of the refractive index of the resonator. In that case, due

#87210 - $15.00 USD Received 4 Sep 2007; revised 12 Nov 2007; accepted 12 Nov 2007; published 21 Nov 2007

to the subsequent growth of the electromagnetic energy inside the cavity, the value of ω_c will be shifted towards ω_p, leading to an increase in the transmission through the system (see red arrow in Fig. 2(a)). Taking into account that this shift $\delta\omega$ is proportional to δn and that, in turn, $\delta n \propto P_{out}$ (since P_{out} is proportional to the energy stored in the cavity), we deduce that $\delta\omega \propto P_{out}$ and consequently that the dependence of P_{out}/P_{in} on P_{out} has also a Lorentzian shape (as shown in Fig. 2(b)). In fact, casting this logic in terms of equations, and starting from Eq. (1), it can be rigorously shown using perturbation theory arguments [19] that this nonlinear dependence can be expressed as the following Lorentzian

$$\frac{P_{out}}{P_{in}} = \frac{1}{1+(P_{out}/P_0-\Delta)^2} \tag{2}$$

where P_0 is the so-called characteristic power of the cavity (this magnitude will be discussed in more detail below) and Δ is the frequency detuning normalized by the width of the resonance, $\Delta = (\omega_c - \omega_p)/\Gamma$. Figure 2(b) displays P_{out}/P_{in} as a function of P_{out} for Δ=3.

Now, if instead of plotting P_{out}/P_{in} as a function of P_{out} we plot P_{out} versus P_{in}, we obtain the dependence shown in Fig. 2(c), where we have considered several values of Δ, ranging from Δ=1 to Δ=3. As can be observed in this figure, for large enough values of Δ (more precisely for $\Delta > \sqrt{3}$), the dependence between P_{out} and P_{in} shows a hysteresis loop (whose unstable branch for each Δ is represented by dotted lines in Fig. 2(c)). Also note that the width of the loop increases with Δ. The bistable loops shown in Fig. 2(c) can be used as the basis for a broad range of applications, such as logical gates or memories (although the response of the materials that form the structure is instantaneous, the nonlinear response of the whole system remembers the past state of the system). Another crucial feature that can be deduced from Fig. 2(c), is that, for a fixed value of the detuning parameter Δ, the operating powers of the system will be determined by the value of the characteristic power P_0. By using perturbation theory arguments [19], it can be rigorously demonstrated that P_0 should scale as $\Gamma^2 V_{MODE}/n_2$ (or equivalently $P_0 \propto V_{MODE}/(Q^2 n_2)$). Actually, this scaling of P_0 in terms of various relevant physical parameters can be also deduced by physical arguments as follows. First of all, from the fact that the frequency should be shifted by more that the cavity resonance width Γ to observe an important change in the transmission through the system, we expect P_0 to be proportional to a factor of Γ. In addition, we expect P_0 to be proportional to another factor of Γ because there are field enhancement effects inside the cavity. P_0 should also depend on the modal volume V_{MODE} [45], since, for a given value of the input power, the induced change of the refractive index inside the cavity δn is inversely proportional to V_{MODE}. Finally, it is clear that P_0 must also be inversely proportional to n_2, since the characteristic power of the system will decrease as the nonlinearity of the considered material becomes larger.

For most conventional nonlinear optical resonators based on Fabry-Perot configurations, the values of Γ and V_{MODE} correspond to power levels well above the threshold $\sim$ 1mW desired for integrated optical devices (e.g. in telecommunication applications). In order to overcome this limitation, it is necessary to look for completely new approaches in the design of the resonator. This is where PhC microcavities come into play. They are ideal candidates to solve this problem, as they are intrinsically characterized by high quality factors and tiny modal volumes (i.e., $Q/V_{MODE} >> 1/\lambda^3$). This unique combination is enabled by the photonic bandgap mechanism, which reflects light without loss and can confine light in an volume smaller than a cubic wavelength.

To illustrate this point, consider the structure displayed in Fig. 3(a). It is formed by a two-dimensional (2D) PhC composed by high-ε dielectric rods embedded in a low-ε dielectric material. A defect has been introduced at the center of the structure by slightly increasing the size of one of the rods. This central defect is coupled symmetrically to two single mode PhC waveguides on the left and right [19]. If we assume that the central rod is made by a

#87210 - $15.00 USD Received 4 Sep 2007; revised 12 Nov 2007; accepted 12 Nov 2007; published 21 Nov 2007

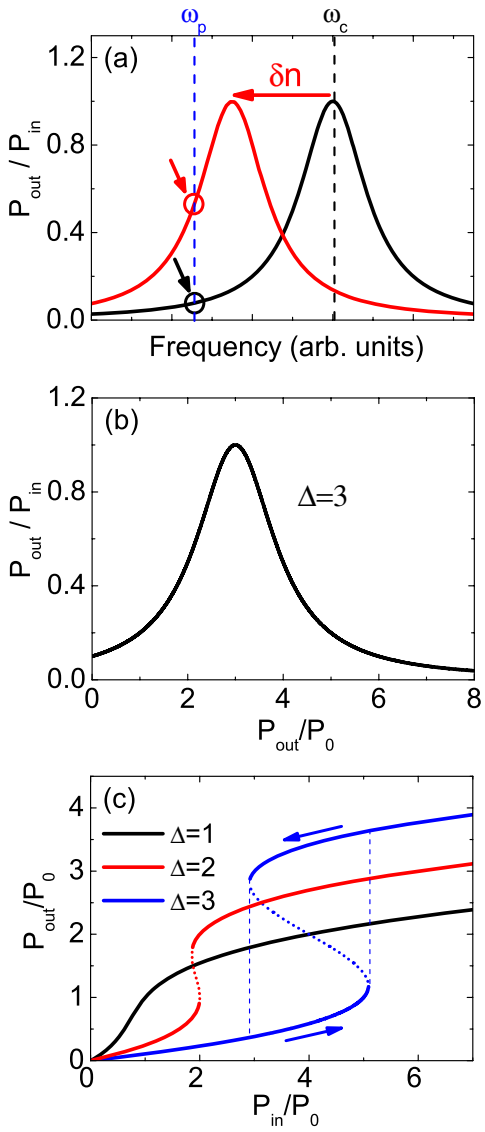

Fig. 2. (a) Evolution of the transmission spectra through the system sketched in Fig. 1 when the refractive index of the resonator is increased by δn. As can be seen in this panel, δn shifts the original resonant frequency of the cavity ω_c (dashed line) towards the frequency of the external illumination ω_p (blue dashed line). (b) Dependence of P_{out}/P_{in} as a function of the outgoing power for Δ=3 (see text for details on this magnitude). (c) Same function as (b) but this time P_{out} is plotted as a function of P_{in} for several values of Δ. Dotted lines display the unstable branches of the hysteresis loop for each case.

Kerr-nonlinear material, this structure can be considered to be a PhC implementation of the system sketched in Fig. 1. Thus, this structure displays the same kind of bistability properties described previously: if we send light through a PhC waveguide, the input–output relation will exhibit bistability (two stable solutions for a given input power), provided that the frequency

#87210 - $15.00 USD Received 4 Sep 2007; revised 12 Nov 2007; accepted 12 Nov 2007; published 21 Nov 2007

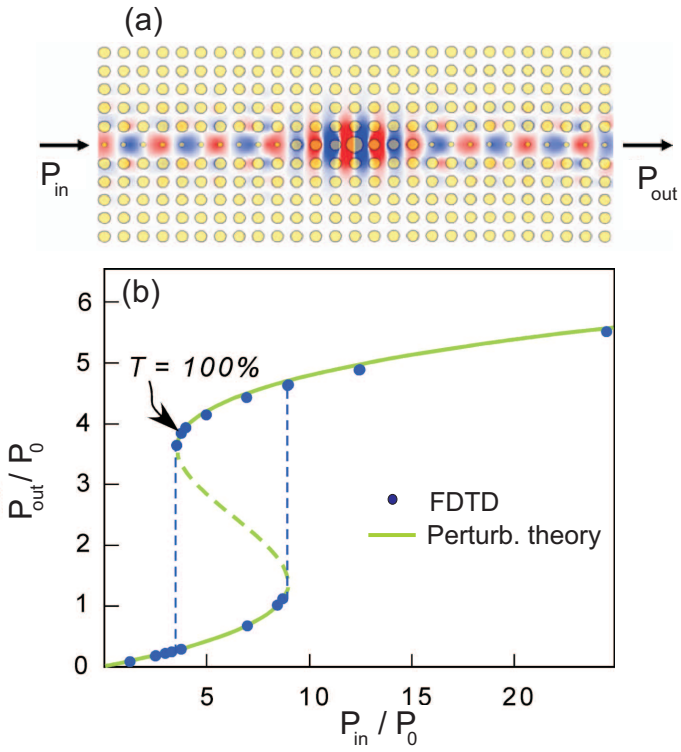

Fig. 3. (a) Photonic crystal implementation of the system sketched in Fig. 1. The PhC is made by a periodic two dimensional distribution of high dielectric rods (ε_H=12.25, yellow regions in the figure) in a low-ε background (ε_L=2.25). The rods have a radius of r=0.25a. A point defect, introduced by increasing the radius of the central rod to r=0.33a, is symmetrically coupled to two single mode PhC waveguides on the left and right. The electric field pointing into the page is depicted with positive (negative) values in red (blue). (b) Computed dependence of the output power (P_{out}) as a function of the input power (P_{in}) for the structure shown in panel (a) when the central rod is assumed to be made by a nonlinear Kerr-like material. Green line displays the results obtained from a perturbation theory analysis while the blue dots correspond to the result of a nonlinear FDTD simulation. Dashed lines represent the unstable branch of the bistable loop.

detuning of the external illumination and the resonant cavity frequency is large enough. This is confirmed by the numerical calculations shown in Fig. 3(b), where the results obtained from both perturbation theory and the nonlinear FDTD method have been plotted (see green line and blue dots, respectively). In this case it has been assumed $\Delta = 3.8$. The crucial point is that although the quality factor shown in Fig. 3(a) is just 500, similar cavities can be designed to show $Q \sim 10^6$ (for instance, just by increasing the number of layers surrounding the defect), while they are confining light in regions of subwavelength size, something that could not be reached in a straightforward manner by using conventional Fabry-Perot devices. This, taking into account the scale law for the characteristic power P_0 we have deduced above, can lead to a reduction of the typical values of P_0 by several orders of magnitude.

Recently, this dramatic decrease of the characteristic power of optical bistability loops has been confirmed experimentally in silicon PhC microcavities [31–33]. In particular in Ref [32] a

#87210 - $15.00 USD Received 4 Sep 2007; revised 12 Nov 2007; accepted 12 Nov 2007; published 21 Nov 2007

microcavity was introduced into a silicon slab with a triangular pattern of air holes by creating a structural point defect in the system. This defect mode had $Q \sim 10^4$ and a modal volume smaller than λ^3. In the experiment reported in Ref. [32], the input and output ports were implemented by means of two PhC defect waveguides coupled to the left and right of the microcavity. Importantly, these experimental results showed that it is possible to find bistability with switching powers as low as 0.4mW, with a values for the pulse energy and switching time of about 70 fJ and 100 ps, respectively.

At this point, let us mention that, in contrast to conventional electronic logical gates, in which most of the operating power is dissipated, in the scheme analyzed in this Section only a small fraction of this power is absorbed by the structure (typically only $\sim 10\%$ of the operating power is absorbed [46], i.e., 7 fJ in the system analyzed in [32]). If we take into account that the energy employed to operate this kind of photonic logical gates can be reutilized in some other parts of the system, it can be stated that the performance of these structures start being comparable to that corresponding to their electronic counterparts (in which the typical value of the power consumed in a single logical gate of modern day microprocessors is of the order of 1 fJ) . Thus, these results challenge the traditional belief that all-optical logic processing based on nonlinear optical devices is not feasible due to the weak nonlinearities of naturally existing materials.

Summarizing, it has been shown that, due to their unique light confinement mechanism, PhC microcavities are particularly suitable for geometric enhancement of nonlinearities. In addition, optical bistability of PhC microcavities can be used as the basis of complex devices performing all-optical logical operations, such as integrated optical isolation [22], logical AND gates [25] and all-optical transistor action [25, 33]. Importantly, due to their characteristic size, switching time and high integrability, this new class of optical processing devices (and similar approaches [47]) have many of the desired features for their on-chip implementation. Thus, we believe that the results reviewed in this section will pave a way to the future optical integrated devices based on enhanced nonlinearities inside PhC microcavities.

3. Harmonic generation in photonic crystal cavities

Nonlinear optical processes can lead to *harmonic generation*, in which light at one frequency ω is converted to light at some multiple of this frequency; for example, a $\chi^{(3)}$ (Kerr) nonlinearity in which the material polarization has a term $\sim E^3$ that leads to generation of 3ω from ω. This process, along with the related processes of sum- and difference-frequency generation ($\chi^{(2)}$) or four-wave mixing ($\chi^{(3)}$), can be exploited for frequency conversion of signals and sources. Just like optical bistability and other topics discussed earlier, the key questions are for what *power* and what *bandwidth* one can achieve efficient frequency conversion. And just like for bistability, the power requirements at a given bandwidth can be greatly decreased by confining light for a long time in a small cavity.

The most basic approach to harmonic generation involves two propagating modes interacting through a nonlinear medium, usually via a $\chi^{(2)}$ (Pockels) or $\chi^{(3)}$ (Kerr) nonlinearity [1, 41, 48–54]. In this case, light at one frequency co-propagates with the generated light at the harmonic frequency. This scheme poses a series of challenges. First, because each field accumulates a different phase as it travels through the waveguide or medium, a phase-matching condition between the two wavelengths must be satisfied in order for the two modes to couple efficiently [55, 56]. Second, the pump power required to achieve maximum nonlinear conversion can be quite high. Instead one employs a cavity to trap the light at the input frequency and/or the output frequency, and it turns out that not only does this greatly reduce the power requirement, but it can also enable 100% conversion in principle. The most common scheme is a singly-resonant cavity, in which the input frequency is trapped and the harmonic frequency immediately escapes, so that all of the light is eventually converted if the lifetime is long enough,

#87210 - $15.00 USD Received 4 Sep 2007; revised 12 Nov 2007; accepted 12 Nov 2007; published 21 Nov 2007

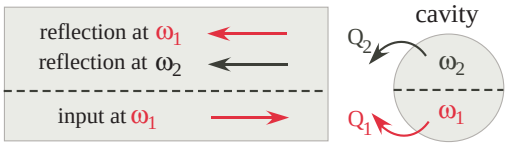

Fig. 4. Schematic diagram of waveguide-cavity system. Input light from a waveguide (left) at one frequency ω_1 is coupled to a doubly-resonant cavity (with resonances at ω_1 and ω_2, with respective lifetimes Q_1 and Q_2) and converted to a cavity mode at another frequency ω_2 by a $\chi^{(2)}$ process. The converted light is radiated back into the waveguide at both frequencies.

and negligible down-conversion occurs [27, 57–74]. A tantalizing possibility, however, is to use a doubly-resonant cavity [35], in which the nonlinear interaction is enhanced by trapping both the input and the harmonic frequencies. In this case, both up- and down-conversion of the frequency must be included, but it turns out that there is a critical pump power (much lower than the power for a singly resonant cavity) at which 100% conversion can be achieved.

As for bistability, the two important quantities that will determine the strength of the nonlinear interactions in the cavity are the lifetime Q and an effective modal volume (represented by V_{HG}). Intuitively, the longer the lifetime (the narrower the bandwidth), the longer the time the light has to interact with the material; similarly, the smaller the modal volume, the more intense the fields are for the same power, and thus the stronger the nonlinear interaction.

In harmonic generation, one can define a modal volume V_{HG} that reflects the spatial extent and overlap of modes at frequencies ω and 2ω (roughly, it can be stated that V_{HG} is a modal volume but one that also depends on the field overlaps). A coupling coefficient, controlling the efficiency of harmonic conversion, is inversely proportional to this quantity, as can be precisely defined using perturbative methods [35], but here we restrict ourselves to scaling arguments for the sake of developing physical intuition. The advantage of using photonic crystals in this context is, just as for bistability, that they allow one to simultaneously achieve high Q and tightly-confined small modal volumes (whose symmetry and field patterns can be precisely controlled), although doubly resonant cavities are a challenge because they require confinement at two very different frequencies. The following discussion is generic to all harmonic generation in cavities, regardless of the specific geometry or confinement mechanism.

We now turn to the details of enhanced nonlinear conversion in cavities by focusing first on the particular case of $\chi^{(2)}$ nonlinearities. It can be shown that in a single-resonant cavity the critical power P_{in} required for high conversion efficiency scales as V_{HG}/Q [75] (note that the scaling of P_{in} is similar to that corresponding to the critical power P_0 defined in the former Section). However, in a doubly-resonant nonlinear cavity, in addition to the coupling coefficients between the two fields ($\sim 1/V_{HG}$), the important figures of merit are the lifetimes Q_1 and Q_2 at the frequencies ω_1 and $\omega_2 = 2\omega_1$, respectively, as depicted schematically in Fig. 4. As shown in [35], in this case, P_{in} scales as $V_{HG}/Q_1^2 Q_2$ (actually, the singly-resonant cavity can be considered as a special case of small Q_2). The additional factor of Q_2 plays a crucial role in decreasing the critical power. For example, for a singly resonant macroscopic cavity displaying second-harmonic generation at $P_{\text{in}} = 1$W operating at a bandwidth $Q \sim 1000$, one can immediately reduce this operating power to milliwatt levels and by further reducing V_{HG} to microscopic sizes, one can in principle obtain microwatt levels [35]. Full expressions for operating powers are obtained by solving explicit coupled-mode equations for the cavity modes [35].

Although it is clear that double resonance should improve harmonic generation, it may not be clear whether 100% conversion may be attained due to the phenomenon of *down-conversion*: as soon as the cavity has accumulated significant energy at both ω_1 and ω_2, difference-frequency

#87210 - $15.00 USD Received 4 Sep 2007; revised 12 Nov 2007; accepted 12 Nov 2007; published 21 Nov 2007

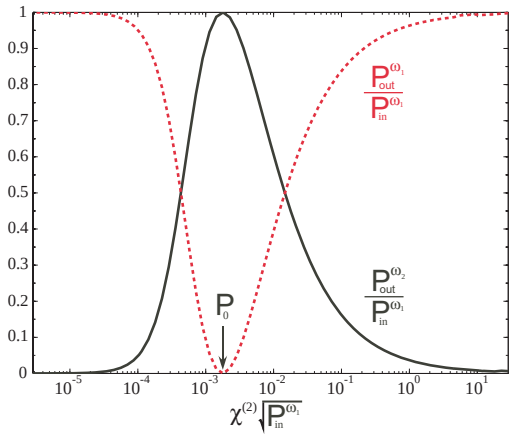

Fig. 5. Plot of conversion efficiency $P_{\text{out}}^{\omega_2}/P_{\text{in}}$ (black), and reflection $P_{\text{out}}^{\omega_1}/P_{\text{in}}$ vs. P_{in} for the schematic geometry in Fig. 4 (Here $P_{\text{in/out}}^{\omega}$ denotes input/output power at frequency ω). The maximum conversion efficiency is achieved at the expected critical power P_0. To compute this figure, we have chosen conservative modal parameters $\omega_1 = 0.3\ 2\pi c/a$, $Q_1 = 10^4$, $Q_2 = 2Q_1$, $1/V_{HG} \approx 10^{-5}a^{-3}$ (where a is the characteristic length scale of the system, see Ref. [35] for further details on this calculation).

generation results in conversion from ω_2 back to ω_1. However, this turns out to be closely related to the problem of *resonant transmission* through cavities: as already seen for the bistable case, when you pump a cavity from one side and the light can either escape back (reflect) or forward into some other channel, 100% transmission (0% reflection) occurs when the cavity decay rates into the two channels are exactly matched. (This is somewhat analogous to "impedance matching.") In the harmonic-generation case, we have a cavity with a single input/output channel that can operate at two frequencies: we are pumping the ω_1 mode from one input channel, and the light can either reflect at ω_1 (either directly or via down-conversion) or be converted and escape at ω_2. So, just as for resonant transmission, we have two escape "channels" and it turns out that we can achieve 100% conversion if we can exactly balance the net reflection rate with the net conversion/escape rate. Here, however, the conversion rate depends upon the *power* as well as on the cavity geometry. If the power is too low, then the nonlinear conversion rate is too small and all the light is reflected at ω_1; this is not surprising. Perhaps more surprisingly, if the power is too *large*, the nonlinear conversion rate is too *big* and all of the harmonic light down-converts and escapes at ω_1. In between these two extremes, there is a *critical power* P_0 where the rates are exactly matched and 100% of the input light is converted and escapes at ω_2 (in the absence of other losses) [35]. It is this critical power that turns out to be proportional to $V_{HG}/Q_1^2Q_2$ [35]. A plot of the numerical conversion efficiency, computed via the coupled-mode equations for a system of the type depicted in Fig. 4, is shown in Fig. 5, and displays precisely the 100% conversion peak at P_0 described above. Furthermore, note that in the example above, conversion efficiencies of 80% or more are predicted over a power P_{in} range of one order of magnitude.

Similar phenomena occur if one considers third-harmonic generation in a doubly resonant $\chi^{(3)}$ cavity, with cavity frequencies ω_1 and $\omega_3 = 3\omega_1$ and corresponding Q values Q_1 and Q_3. (It is also possible to perform third-harmonic generation via a $\chi^{(2)}$ medium, using a combination of second-harmonic and sum-frequency generation [72,76]). Again, there is a coupling coefficient $\sim 1/V_{HG}$. Again, there is a critical power P_0 where 100% conversion is possible, by matching the conversion and reflection rates.Here, the critical power $P_0 \sim V_{HG}/(Q_1^{3/2}Q_3^{1/2})$, which for

#87210 - $15.00 USD Received 4 Sep 2007; revised 12 Nov 2007; accepted 12 Nov 2007; published 21 Nov 2007

$Q_1 = Q_3$ gives a similar figure of merit as that found in the bistability case V_{HG}/Q^2.

All of these statements can be precisely derived from perturbation and coupled-mode theory [35]. However, $\chi^{(3)}$ media introduce an additional wrinkle: *self-phase modulation* (SPM), where the nonlinearity shifts the cavity frequencies in addition to generating the harmonic. In the bistability phenomenon, SPM was the source of the entire effect, but here it poses a problem because, as the input power is increased, the cavity frequencies shift out of resonance. This shift can be countered by appropriately detuning the cavity frequencies beforehand [35].

4. Tailoring optical nonlinearities via the Purcell effect

In this section, the impact of the Purcell effect upon the strength of the Kerr nonlinear coefficient is discussed. The Purcell effect, first discovered in 1946 [77], is a phenomenon whereby a complex dielectric environment strongly enhances or suppresses spontaneous emission (SE) from a dipole source [78–81]. Recently, it was shown that using the Purcell effect for frequencies close to an atomic resonance can substantially influence the resultant Kerr nonlinearity for light of all (even highly detuned) frequencies [36].

Optical nonlinearities are caused by atomic or molecular resonances: the closer the frequency ω becomes to the resonant frequency ω_{ba}, the stronger the atom-photon coupling becomes and the larger the nonlinear effects. On the other hand, operating too close to resonance generally leads to large absorption loss, so instead one operates at a *detuned* frequency $\omega = \omega_{ba} + \Delta$. Intuitively, modifying the SE rate of the resonance changes a property of the resonance which causes nonlinearity, so it should modify the nonlinear process in some way. The key point is that the atomic resonance and the optical mode lie at different frequencies: this makes it possible for a photonic crystal to *suppress* SE at ω_{ba} via a photonic band gap, which *increases* $\chi^{(3)}$ as shown below, while simultaneously operating at a probe frequency ω outside the gap. In fact, one can additionally simultaneously engineer *optical* resonant cavities at ω, which further enhance nonlinear effects by concentrating the fields.

Moreover, as we show below, this enhancement effect displays some unexpected properties. For example, while increasing SE strengthens the resonance by enhancing the interaction with the optical field, it actually makes the optical nonlinearity weaker. Furthermore, phase damping (e.g., through elastic scattering of phonons), which is detrimental to most optical processes, plays an essential role in this scheme, because in its absence, these effects disappear for large detunings (i.e., the regime in which low loss switching can take place).

In order to approach this problem quantitatively, we start with a simple, generic model displaying Kerr nonlinearities: a collection of two-level systems. The corresponding complex Kerr susceptibility has been calculated in the steady state limit using the rotating wave approximation [1, 36, 82], and is given by:

$$\chi^{(3)} = \frac{4}{3} N \mu^4 \frac{T_1 T_2^2 (\Delta T_2 - i)}{\hbar^3 (1 + \Delta^2 T_2^2)^2}, \tag{3}$$

where N is the number of two-level systems, μ is their dipole moment, T_1^{-1} is the rate of population decay, $T_2^{-1} = \left[(1/2)T_1^{-1} + \gamma_{\text{phase}}\right]$ is the rate of phase damping, and $\Delta \equiv \omega - \omega_{ba}$ is the detuning of the incoming wave of frequency ω from the electronic resonance frequency ω_{ba}. For large detunings $\Delta T_2 \gg 1$, one obtains the approximation that:

$$\mathrm{Re}\,\chi^{(3)} \approx \frac{4}{3} N \mu^4 \left(\frac{1}{\hbar\Delta}\right)^3 \frac{T_1}{T_2}. \tag{4}$$

Of course, there are many types of materials to which a simple model of noninteracting two-level systems does not apply. However, it has been shown that $\chi^{(3)}$ nonlinearities of some

#87210 - $15.00 USD Received 4 Sep 2007; revised 12 Nov 2007; accepted 12 Nov 2007; published 21 Nov 2007

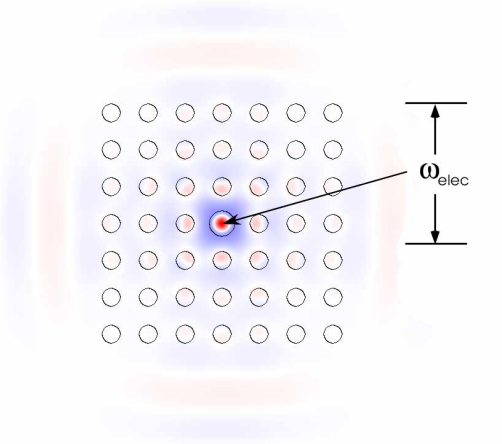

Fig. 6. A 7x7 square lattice of dielectric rods ($\varepsilon = 12.25$) in air, with a single defect rod in the middle. On top of the dielectric structure outlined in black, the E_z field is plotted, with positive (negative) values in red (blue). A small region of nonlinear material, e.g., a CdSe nanocrystal, with transition frequency ω_{elec}, is placed in the defect rod.

semiconductors such as InSb (a III-V direct bandgap material) can be treated as a collection of independent two-level systems with energies given by the conduction and valence bands, and yield reasonable agreement with experiment [83]. The predicted nonlinear coefficient displays the same scaling with lifetimes as Eq. (4), so the considerations that follow should also apply for such semiconductors.

Now, consider the effects of changing the SE properties for systems modeled by Eq. (4), in which $\chi^{(3)}$ scales as T_1/T_2. Oftentimes, the phase coherence time T_2 will be much smaller than T_1 [84], so that $T_2 \approx \gamma_{\text{phase}}^{-1}$ will remain nearly unchanged even if T_1 is altered by the Purcell effect. In that case, the enhancement of the real part of $\chi^{(3)}$, denoted by η, will be given by $\eta \approx T_{1,\text{purcell}}/T_{1,\text{vac}}$, which means that the suppression of SE will enhance nonlinearities. This comes about because a larger T_1 increases the virtual lifetime for nonlinear processes to occur [85]. Conversely, Purcell enhancement suppresses nonlinearities by reducing this virtual lifetime.

The rate of phase damping is crucial to this scheme, because as in the limit that phase damping is controlled exclusively by the SE rate (i.e., $T_2 \approx 2T_1$), the ratio T_1/T_2 in Eq. (4) will not be altered by changes in SE, and therefore, the nonlinearity will revert to its normal value for large detunings (i.e., the regime in which lossless switching can take place).

It is also interesting to note that this enhancement scheme will generally not increase nonlinear losses, which are a very important consideration in all-optical signal processing. If the nonlinear switching figure of merit ξ is defined by $\xi = \text{Re}\,\chi^{(3)}/(\lambda\,\text{Im}\,\chi^{(3)})$ [86], then $\xi_{\text{purcell}}/\xi_{\text{vacuum}} = T_{2,\text{purcell}}/T_{2,\text{vacuum}} \geq 1$, for all cases of suppressed SE.

The general principle described thus far should apply for any medium where the local density of states (DOS) is substantially modified provided that one is in the weak-coupling regime [87]. In the following, we show how this effect would manifest itself in a PhC system, thus illustrating how strong nonlinear suppression or enhancement effects could be achieved in practical physical systems. Our system consists of a seven by seven 2D square lattice of dielectric rods ($\varepsilon = 12.25$ and radius $0.25a$) in air, with a two-level system placed in the middle defect rod of radius $r = 0.35a$, as illustrated in Fig. 6.

First, consider the magnitude of the enhancement or suppression of SE in this system.

#87210 - $15.00 USD Received 4 Sep 2007; revised 12 Nov 2007; accepted 12 Nov 2007; published 21 Nov 2007

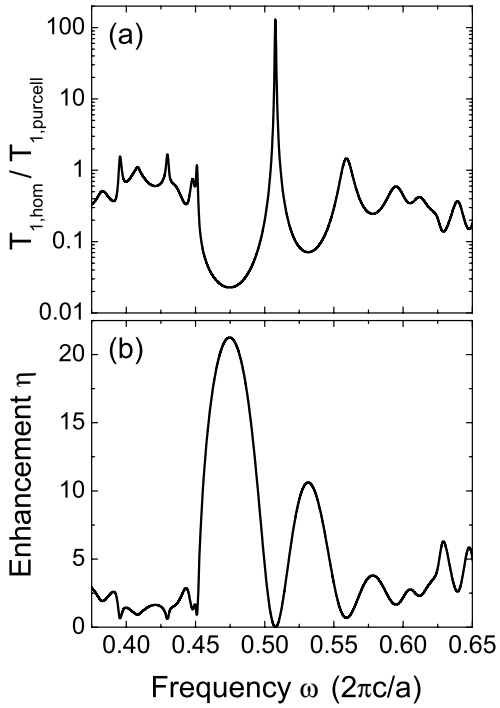

Fig. 7. (a) Numerical calculation of the enhancement of SE for the set-up in Fig. 6, given by the ratio of the rate of emission in the PhC, $T_{1,\text{purcell}}^{-1}$, divided by the emission rate in vacuum, $T_{1,\text{vac}}^{-1}$. (b) Kerr enhancement $\eta \equiv \text{Re}\,\chi_{\text{purcell}}^{(3)}/\ \text{Re}\,\chi_{\text{vac}}^{(3)}$ as a function of electronic transition frequency (ω_{elec}) for a system of dielectric rods in air, with the parameter values listed in the text.

Clearly, since there are several periods of high contrast dielectric, one expects to observe two distinct effects. First, there will be a substantial but incomplete suppression of emission inside the bandgap. Second, there will be an enhancement of SE outside the bandgap (since the DOS is shifted to the frequencies surrounding the bandgap), and also close to the cavity resonance. For an atom polarized in the direction out of the 2-D plane, only the TM polarization need be considered. The enhancement of SE obtained in a time-domain simulation is plotted in Fig. 7(a).

Some recent work has demonstrated that single nanocrystals can demonstrate predominantly radiative decay in vacuum even at room temperature, e.g., single CdSe/ZnS core-shell nanocrystals with a peak emission wavelength of 560 nm have $\Gamma_{\text{rad}} \approx 39\Gamma_{\text{nr}}$, where the radiative lifetime $T_{1,\text{rad}} = 25.5$ ns [88]. Extrapolating from low temperature results [89], we estimate $T_2 \approx 0.13$ fs at room temperature.

When these data are combined with the data from Fig. 7(a), we can calculate the enhancement of the real part of the Kerr coefficient, η, as a function of the atomic transition frequency ω_{elec}, when probed at a frequency $\omega_{\text{ph}} = 0.508(2\pi c/a)$ (the cavity's resonant frequency). The results are shown in Fig. 7(b). Enhancements of up to a factor of 21 are predicted in the regions in which SE is suppressed, for these exact parameter values. This set-up has the advantage of allowing simultaneous probe field enhancement (through the concentration of the field in the defect mode), along with nonlinear coefficient enhancement (through the suppression of spontaneous emission). The enhancement factor is less than the theoretical maximum value of 40 obtained from the expression for maximum nonlinear enhancement that takes the quotient

#87210 - $15.00 USD Received 4 Sep 2007; revised 12 Nov 2007; accepted 12 Nov 2007; published 21 Nov 2007

of T_1 values with and without complete SE suppresion for this material because the SE is suppressed only by a factor of about 43, as shown in Fig. 7(a). However, a much bigger PhC, which suppresses SE very strongly, should approach the theoretical maximum enhancement. If a single nanocrystal with the parameters above proves difficult to use in practical devices, note that even bulk samples of similar nanocrystals have been shown to yield a significant radiative decay component, corresponding to $\Gamma_{rad} \approx \Gamma_{nr}$ [90]. Thus, it has been predicted that with strong suppression of radiative decay, nonlinear enhancement of a factor of two or more could be observed at room temperature, for certain materials.

We now discuss the implications of this effect on the results discussed earlier in this review. Most past experiments should not have observed this effect, because they were designed with photonic bandgaps at optical frequencies significantly smaller than the frequencies of the electronic resonances generating the nonlinearities, in order to operate in a low-loss regime. Furthermore, in most materials, non-radiative decays will dominate radiative decays at room temperature. Finally, all the previous *analyses* are still valid as long as one considers the input parameters to be effective nonlinear susceptibilities, which come from natural nonlinear susceptibilities modified in the way described by this paper.

Summarizing, it has been shown that the Purcell effect can be used to tailor optical nonlinearities [36]. We have illustrated in an exemplary system how enhancements of Kerr nonlinearities of at least one order of magnitude should be achievable. This phenomenon is caused by strong modification of the local DOS near the resonant frequency. Thus, our treatment can easily be applied to analyze the Kerr nonlinearities of two-level systems in almost any geometrical structure in which the Purcell effect is substantial (e.g., PhC fibers [91] or optical cavities). It also presents a reliable model for a variety of materials, such as quantum dots, atoms, and certain semiconductors. Finally, note that the physical principle described in this Section (i.e., the strong modification of nonlinearities via the Purcell effect) should have a general character, and thus may apply to coefficients at other orders, such as $\chi^{(5)}$, and to other materials (e.g. where two-level approximation does not apply).

5. Summary and conclusions

Photonic crystal microresonators offer a unique mechanism for confining light, giving rise to a combination of high quality factors and small modal volumes. This puts many previously known nonlinear optical processes in a new operating regime. For example, we have shown that optical bistability is greatly amplified in these systems. Also second and even potentially third harmonic generation can be made to operate with high efficiences with resonances at both the input and output frequencies, up to 100 % efficiency at a particular, low input power. Finally, the Kerr coefficient itself has been shown to be capable of being tailored via careful modification of the radiative properties of the nonlinear medium.

In summary, all these phenomena have already begun to enable the design of novel all-optical signal processing devices whose operating powers and switching times are orders of magnitude smaller than those corresponding to traditional nonlinear optical devices. These properties, combined some other key features of these devices, such as their micrometric size and their high integratibility, could make nonlinear photonic crystal cavities one of the most important actors in the development of future photonic integrated technology.

Acknowledgements

This work was supported in part by the Materials Research Science and Engineering Center Program of the National Science Foundation under Grant No. DMR 02-13282, the Army Research Office through the Institute for Soldier Nanotechnologies Contract No. W911NF-07-D-0004, and the U.S. Department of Energy under Grant No. DE-FG02-99ER45778.

#87210 - $15.00 USD Received 4 Sep 2007; revised 12 Nov 2007; accepted 12 Nov 2007; published 21 Nov 2007